nature energy

Article

https://doi.org/10.1038/s41560-026-01990-2

A cation-functionalized layer for ethylene electrosynthesis via CO reduction paired with H_2 oxidation in a pure-water-fed solid-state electrolyser

Received: 12 May 2025

Accepted: 20 January 2026

Published online: 17 February 2026

Check for updates

Bosi Peng[1,2,4], Zeyan Liu[1,2,4], Xiangyu Ma[1,4], Weiyan Ni[1,2], Aamir Hassan Shah[1], Charles B. Musgrave III[1], Hyundo Park[1], Jin Huang[1], Aditya Menon[1,3], Mercouri G. Kanatzidis[1], Ke Xie[1,2] ✉ & Edward H. Sargent[1,2] ✉

As industrial demand for electricity grows, the high energy cost of electrifying chemical production is of further-increased concern: the most efficient oxygen-evolution-coupled ethylene electrosynthesis system requires >130 $GJ_{electricity}$ per ton of C_2H_4 and is limited to <10-hour stability when powered using intermittent electricity. Here we pursued ethylene electroproduction employing a more energetic feedstock—syngas—available from thermo-gasification, to reduce electricity consumption of the whole ethylene production process, and we constructed an all-gas-fed system to avoid caustic electrolyte. We identified a key challenge in such a system: when no alkali anolyte was present, known solid-state electrolytes were ineffective in activating the CO-to-ethylene transformation. We therefore explored a suite of candidate ionomers and evaluated codesign for high ion-exchange capacity united with optimized cation binding. We identify polyacrylate as an efficient host that enables C_2H_4 production at 1.2 V and 100 mA cm^{-2} (49 $GJ_{electricity}$ per ton of C_2H_4) in the solid-state system that operates stably for over 80 hours and after 30 on/off cycles when powered using intermittent electricity.

Ethylene (C_2H_4) is a widely used industrial chemical, a building block for plastics, resins, synthetic fibres and an enabler of applications in the automotive and packaging sector[1,2]. In today's industrial process, C_2H_4 is produced through the steam cracking of ethane or naphtha, each reliant on fossil feedstock and emitting ~1 ton of CO_2 (ton_{CO2}) per ton of C_2H_4 (ton_{C2H4}) cradle to gate[3]. Electrochemical systems that couple the reduction of CO_2/CO (CO_2/COR) to C_2H_4 (CO_2/COR:OER) with water oxidation (OER) have been explored to provide prospectively lowered-carbon-intensity pathways when these are powered using renewable electricity (Fig. 1a).

Such processes reduce CO_2 from the atmosphere under mild operating conditions, but they are bounded by a thermodynamic energy floor of 50 GJ per ton_{C2H4} from CO_2 and 30 GJ per ton_{C2H4} from CO (Fig. 1b). The actual electrical energy expended in experimentally implemented electrochemical systems from CO_2 has to date demanded >130 $GJ_{electricity\ per}$ ton_{C2H4} (ref. 4).

In light of ethylene's global production rate of 300 million tons per year (refs. 5,6), the electrification of worldwide C_2H_4 production at the best-reported energy efficiencies would require 1.5 times the total present-day worldwide supply of renewable electricity[7,8]. Across

[1]Department of Chemistry, Northwestern University, Evanston, IL, USA. [2]Department of Electrical and Computer Engineering, Northwestern University, Evanston, IL, USA. [3]Department of Chemical and Biological Engineering, Northwestern University, Evanston, IL, USA. [4]These authors contributed equally: Bosi Peng, Zeyan Liu, Xiangyu Ma. ✉e-mail: ke-xie@northwestern.edu; ted.sargent@northwestern.edu

https://doi.org/10.1038/s41560-026-01990-2

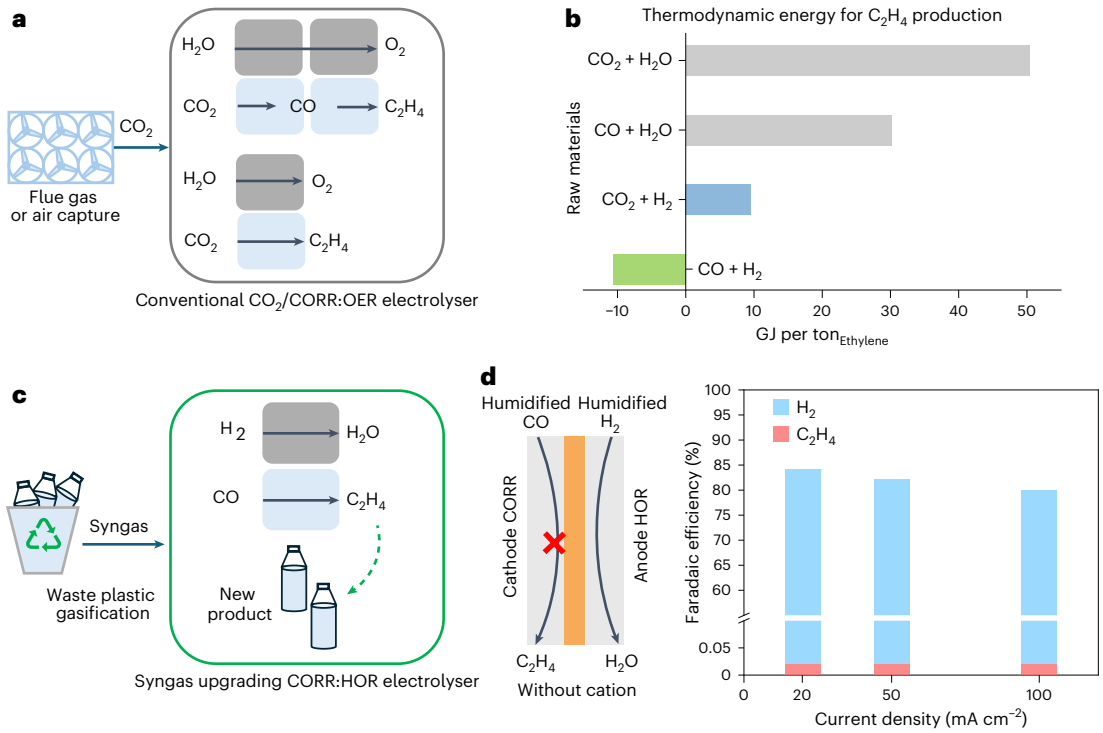

Fig. 1 | Schematics of typical COR electrolysis systems and the solid-state system. a, Ethylene production using CO_2/CO and water as raw material in CO_2/COR:OER system. **b**, Comparison of thermodynamic minimum energy for ethylene production in different systems. **c**, Electrifying ethylene production by upgrading syngas derived from waste plastics in the COR:HOR system. **d**, Schematic of a solid-state COR:HOR system and experimental data on its hydrogen and ethylene FE in a system without liquid anolyte.

industrial sectors, electricity demand is increasing[9], a trend that motivated us to map more electricity-conserving electro-chemo-synthetic routes.

As one means to lower electricity consumption, we contemplated C_2H_4 synthesis from a more energy-rich feedstock, such as syngas that can be generated from plastic waste, biomass and municipal waste gasification[2]. Syngas to ethylene, $2CO + 4H_2 \rightarrow C_2H_4 + 2H_2O$ (Fig. 1c), is in principle exothermic at −10.6 GJ per ton_{C2H4} (Fig. 1b).

Today's syngas-to-ethylene, such as accomplished via Fischer–Tropsch synthesis (FT) and methanol-to-olefins (MTO), suffers from a wide product distribution[10,11]. In the case of MTO, for example, the products are evenly distributed between ethylene and propylene, a ratio ill-matched to relative market demand for C2 vs C3 products[12].

The electrochemical conversion of CO to ethylene has proceeded rapidly and is now producing C_2H_4 with a Faradaic efficiency (FE) exceeding 75% (refs. 4,13). We thus studied here whether we could develop a syngas-fed system, replacing OER with HOR: a COR:HOR coupled electrolysis system (Fig. 1c). As well as decreasing electricity demand, the lower anodic applied potential might increase stability, both of the anode catalyst and of membrane/ionomers[14].

We noted also that COR typically relies on a high-molarity aqueous anolyte, such as NaOH, to provide a high cation concentration and high local pH on the cathode to activate the conversion from CO to C_{2+} products; but that the liquid anolyte permeates the membrane, flooding the cathode-side catalyst layer and gas diffusion electrode. When electricity is intermittent, such as in the case of off-grid solar and wind, the corrosive anolyte degrades the cathode catalyst when it is transiently outside of the cathodic protection regime of high applied reducing bias[15–17].

A fully gas-fed solid-state electrochemical system, such as a COR:HOR system, could avoid aqueous alkaline electrolyte through the use of humidified CO on the cathode and humidified H_2 on the anode. HOR is well optimized in a gas-fed environment, whereas OER suffers greater overpotentials than in liquid anolyte due to the limited reactant concentration[14].

Here we turned our attention to strategies that would provide, in the solid state, the needed cation effects for a fully gas-fed solid-state COR:HOR system. We found that previously reported solid-state electrolyte strategies that have been effective in activating CO_2R—including both organic cation[15,18–20] and alkali cation-exchanged ionomer approaches[21,22]—failed to activate CO to ethylene. We studied the chemistry underpinnings of this failure, and these led us to solid-state functionalized ionomers that activate CO to C_{2+} products, such as ethylene, in a fully gas-fed electrochemical system.

Exploration of cation-functionalized layers to activate COR

We first explored and constructed a humidified-gas-fed solid-state system (Fig. 1d); however, we found that without the alkali cations, the major product is H_2 (FE > 99%). Alkali cations are absent in such pure-water humidified system, and these are known to play a central role on the surface of the cathode catalyst to activate COR to C_2H_4 and to create locally alkaline conditions to suppress H_2 evolution[23–25].

We then implemented cation-functionalized layers in an established COR:OER system (Fig. 2a) and used previously reported ammonium cation groups that had proven effective in CO_2R in pure-water electrolysis: we explored piperidinium[15], imidazolium[18] and benzimidazolium[19,20]. We spray-coated a mixture of carbon nanoparticles and ammonium cation ionomer to form a cation-functionalized layer on the side of the membrane facing the cathode catalyst layer.

Unfortunately, in COR, this approach was not effective, consistently providing $FE_{C2H4} < 5\%$ (Fig. 2b).

We studied the effect of different cation species with the aid of in situ Raman spectroscopy (Supplementary Fig. 1), looking both at COR adsorbates and reaction intermediates (Fig. 2c,d). We focused on Raman features at 1,900–2,200 cm^{-1}, which correspond to C–O

https://doi.org/10.1038/s41560-026-01990-2

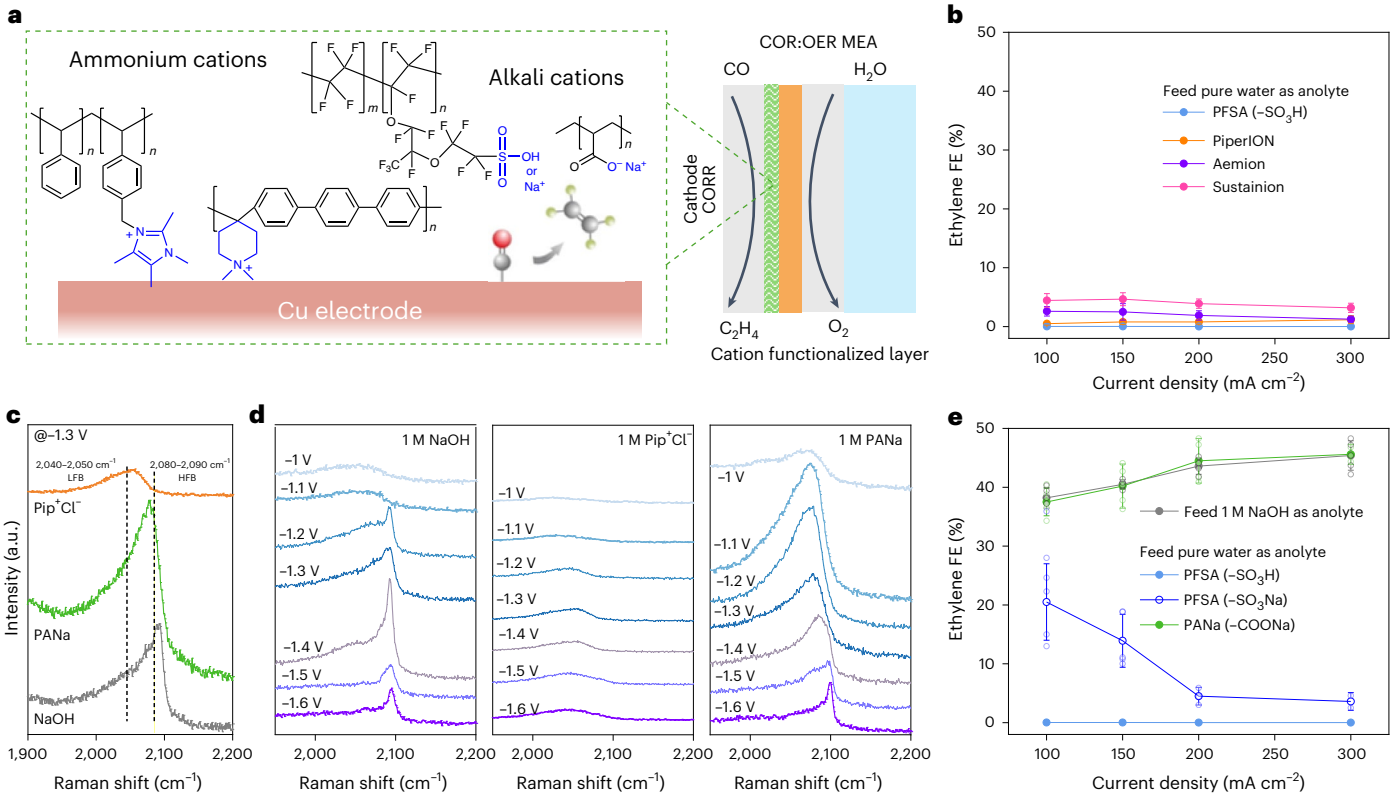

Fig. 2 | A cation-functionalized layer for pure-water-fed conditions. **a**, A cation-functionalized layer applied to a Cu catalyst in a COR:OER system operating with pure water as anolyte. **b**, Comparison of C_2H_4 FE with the system using commercial Cu catalyst under pure water, with and without the introduction of various ammonium cations across different current densities. **c**, In situ Raman spectroscopy at −1.3 V vs Ag/AgCl illustrating the impact of different cation groups on the adsorbed CO species. **d**, In situ Raman spectra of CO characteristic peak at the varying potential (vs Ag/AgCl) in the different electrolytes (1 M NaOH, 1 M Pip^+Cl^-, 1 M PANa). Noted that the surface-adsorbed CO showed only low-frequency band (LFB) in the case of the large cation group (*N*,*N*-dimethyl-piperidinium: Pip^+), while showing similar behaviour under PANa and NaOH. **e**, C_2H_4 FE comparison between commercial Cu catalysts in pure water at varying current density when alkali cations were introduced by cation-grabbing polymers. Data are presented as mean values and the error bars represent standard deviation from at least three independent tests (the individual data points are shown as hollow dots).

stretching of two *CO configurations: low-frequency linear band CO (LFB) at 2,040 cm^{-1} on terraced Cu sites and the high-frequency linear band CO (HFB) at 2,080 cm^{-1} on defective Cu sites[26,27]. The HFB has previously been correlated closely with atop *CO configuration at relatively high CO coverage[27]. We reconfirmed that in systems employing high-molarity NaOH—systems that achieve high FE_{C2H4}—the HFB predominated (Fig. 2c, grey). The HFB-to-total-band-area fraction further increases with more negative potential (Fig. 2d and Supplementary Fig. 2). In contradistinction, in the case of *N*,*N*-dimethylpiperidinium chloride (PiP^+Cl^-), while LFB dominates CO stretching (Fig. 2c, orange) and no HFB peak was observed even with more negative potential while the *CO peak showed notably lower intensity (Fig. 2d and Supplementary Fig. 2). We also reconfirmed that FE_{C2H4} remained below 10% in a flow cell test with 1 M PiP^+Cl^- as catholyte, and we studied (and ruled out experimentally) a major role for the Cl^- ion (Supplementary Fig. 3).

From these observations, we concluded that the ammonium cations—effective in CO_2R (refs. 15,18,19)—were not effective in producing the signatures of COR activation: instead, they led to a lower CO population on the surface compared to the case of alkali metal cations. We offer that this could be because the large size and low charge density of bulky organic cations fail to create the strong interfacial electric field needed to stabilize CO* intermediates for ensuing C–C coupling[28], consistent with the observation of a smaller double layer capacitance for the case of bulky organic cations compared to the case of alkali cations (Supplementary Fig. 4); possible site blocking by the interfacial organic layers, suggested by the emergence of the second semi-circle in the electrochemical impedance spectroscopy (EIS) (Supplementary Fig. 4c), or weakened electrosorption of *CO due to lower surface charge density[29].

We searched therefore for solid-state means to provide alkali cations proximate to the cathode catalyst surface. We turned our attention to ionomers containing negatively charged groups capable of hosting cations, including perfluorinated sulfonic acid (PFSA), which contains sulfonic acid group ($–SO_3H$) terminated side chains[21,30]. We soaked the PFSA in NaOH (Methods) to exchange the proton sites in PFSA with alkali cations (PFSA–SO_3Na). When we fed pure water as anolyte, the FE_{C2H4} rose to over 20% (Fig. 2e, blue), whereas the MEA with non-exchanged PFSA–SO_3H produced solely H_2 (Fig. 2b,e, light blue).

Unfortunately, when we operated the system for less than an hour, the FE_{C2H4} declined (Supplementary Fig. 5), a trend also seen with increased current densities (Fig. 2e), suggesting the limited effectiveness of alkali cation-exchanged PFSA ionomers in elevated current density region and prolonged testing. We note that typical PFSA ionomers have only a modest ion-exchange capacity (IEC) and thus are expected to lead to a limited cation concentration at the interface: this can explain their failure to activate COR and to suppress the unwanted hydrogen evolution reaction (HER). The strong acidic nature of the sulfonate group may produce only limited binding of the cations, leading to cation leaching (Supplementary Table 1).

We considered the attributes of ionomers for a solid-state cation-functionalized layer. In addition to possessing high IEC, the ionomer functional group would need to produce optimal cation

https://doi.org/10.1038/s41560-026-01990-2

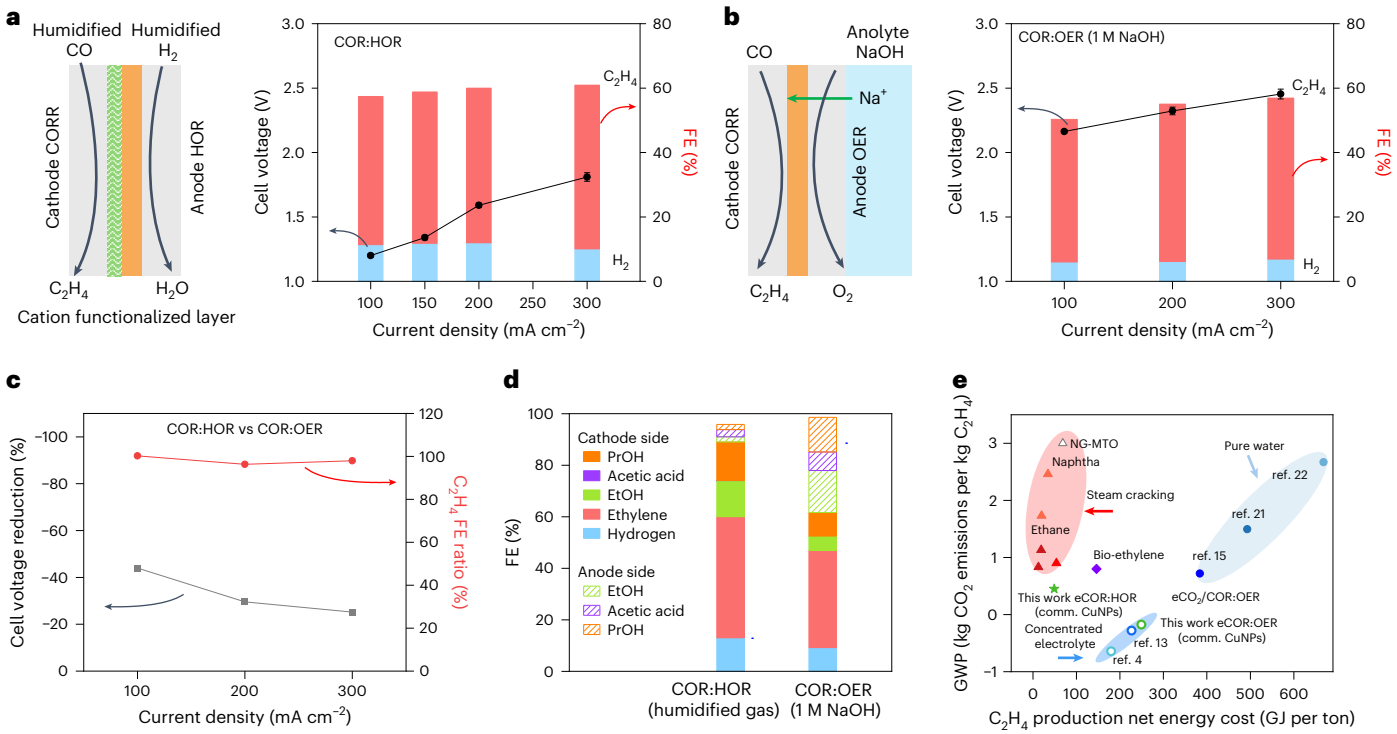

Fig. 3 | Integration of a cation-functionalized layer into a solid-state COR:HOR system. a,**b**, Cell voltage and ethylene FE vs current density for pure-water-fed solid-state COR:HOR MEA (**a**) and conventional COR:OER MEA fed with 1 M NaOH (**b**). The error bars represent the standard deviation from two independent tests. **c**, Cell voltage reduction and C_2H_4 FE comparison between two systems. **d**, Full product analysis, including liquid and gas products. The liquid product crossover (%) was calculated from the ratio of liquid product collected from the anode over total liquid products. **e**, Comparison of carbon footprint and ethylene production net energy cost (only consider the process energy costs: electricity for electrolysers, thermal energies for carbon capture and steam cracking, the heating value of feedstocks and products is not considered) among the eCOR:HOR pure-water-fed system (light blue shade), other state-of-the-art CO_2/COR:OER electrolysers (dark blue shade) and commercial thermal C_2H_4 production routes (red shade).

binding: too weakly bound cations would be leached from the system, whereas overly strongly bound cations may fail to activate COR (Supplementary Fig. 6a). To test this chemical picture, we studied a group of ionomers having a spectrum of cation binding affinities (pK_a values in Supplementary Table 1 and from density functional theory (DFT) in Supplementary Fig. 7).

The results show a trend linking cation binding strength, FE_{C2H4}, stability and alkali cation retention/loss rate (Supplementary Fig. 6). When cation binding is too strong, such as in the case of Na^+-crown ether showing <20% FE_{C2H4}, there is a failure to produce CO activation; when it is too weak, progressive loss of the cation (for example, PFSA case) is observed, such as with an initially impressive ~40% FE_{C2H4} at beginning of life but a rapid ensuing decline of FE_{C2H4}; this linked to a high rate of Na^+ leaching. Sodium polyacrylate (PANa), which has an IEC of 14 milliequivalent per gram and a carboxylic anion host, we selected for further study, for we observed it to exhibit the best binding and overall performance[31] (Supplementary Figs. 6–8). We then moved to employ PANa on support (for example, carbon black; Methods), because PANa on support is known to provide a stable solid-state electrolyte in the allied field of Zn-air batteries[32–34].

In situ Raman spectroscopy in 1.0 M PANa (Fig. 2c,d) showed that the CO adsorption behaviour during COR in the case of PANa is similar to the case of 1.0 M NaOH with similar HFB-dominated CO peak (Fig. 2c, green) and similar potential dependent trend of HFB-to-total-band-area fraction and similar ratio among the various water structures (Fig. 2d and Supplementary Fig. 2). To ensure a reliable correlation between the Raman result and the MEA performance, we further checked the COR performance in flow cell using 1.0 M PANa as catholyte. We obtained a FE_{C2H4} of 44% and H_2 FE suppressed to 10%, comparable to results seen in the MEA system (Supplementary Fig. 9).

When we used PANa as cation-functionalized layer (Methods provide fabrication details) and explored it in COR:OER MEA with pure water as anolyte (Fig. 2a), we achieved FE_{C2H4} of 46 ± 2% (Fig. 2e, green), similar to the 45 ± 3% at 300 mA cm^{-2} value obtained when 1.0 M NaOH is used as anolyte (Fig. 2e, grey). The PANa cation-functionalized layer retained FE_{C2H4} during a 2-hour study, whereas FE_{C2H4} decreased in the case of PFSA–SO_3Na (Supplementary Fig. 7).

Development of a solid-state COR:HOR MEA

We incorporated the cation-functionalized layer into a solid-state COR:HOR MEA electrolyser fed with humidified gases. In this pure-water-fed system with commercial Cu catalyst, we observed a FE_{C2H4} of 50% with a full cell voltage of 1.2 V at 100 mA cm^{-2} (Fig. 3a; full product analysis in Supplementary Fig. 10a). This compared favourably to the 2.2 V seen in COR:OER with similar FE_{C2H4}, especially since this latter was fed with 1.0 M NaOH (Fig. 3b; full product analysis in Supplementary Fig. 10b). Remarkably, whereas a drastic FE drop was reported when moving from the alkaline anolyte system to pure water[35], we observed no loss in FE_{C2H4} in the pure-water-fed system employing a cation-functionalized layer (Fig. 3c). As an added benefit, we collected alcohol products at a concentration of ~1.8 M (Supplementary Fig. 11a,b) from COR:HOR MEA, for these in the present dry system had not suffered dilution in an aqueous electrolyte. This molarity is orders of magnitude higher than what we achieve in the COR:OER configuration, and the system also suffered three times less liquid product crossover, something we assign to the forward-bias AEM:CEM design (Supplementary Fig. 11c and Fig. 3d). In prior related studies, liquid product crossover has led to product oxidation and dilution in concentrated anolyte, militating against energy-efficient product separation[20].

https://doi.org/10.1038/s41560-026-01990-2

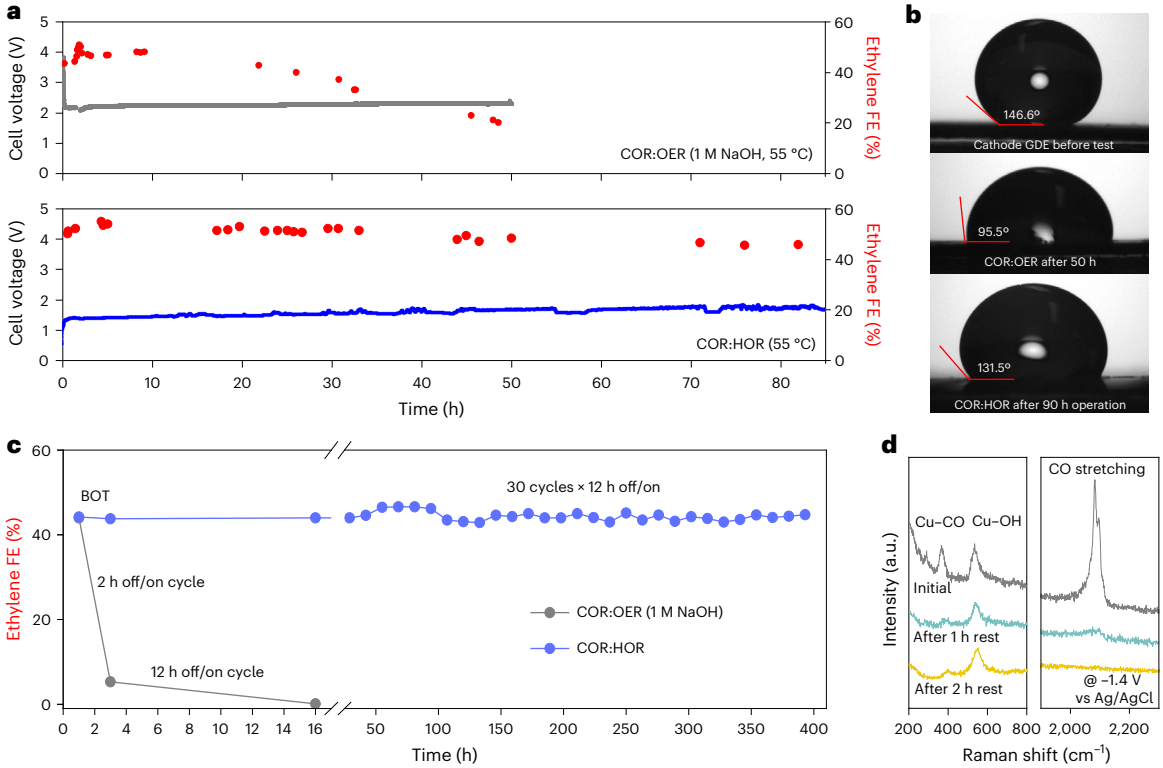

Fig. 4 | Stability under intermittent electricity supply. a,**b**, Comparison of cell voltage and ethylene FE during continuous operation with conventional COR:OER MEA fed with 1 M NaOH (top) and pure-water-fed solid-state COR:HOR MEA (bottom) (**a**), photographs of contact angle measurements on the cathode gas diffusion electrode of COR:OER MEA (top) and COR:HOR MEA (bottom) after stability test (**b**). **c**, FE_{C2H4} of COR:OER and COR:HOR system during multiple on/off cycling with required resting times of (2 hours or 12 hours). The products during operation were analysed when the cell was stabilized. **d**, In situ Raman spectroscopy at −1.4 V vs Ag/AgCl showing the change in adsorbed CO and OH before and after withdrawing reductive potential for 1 h and 2 h.

We assessed the prospective economic feasibility and environmental impact of ethylene production (details in Methods) via pure water COR:HOR syngas upgrade (Fig. 3e, green star) and compared these estimates with industrial thermochemical ethylene production processes (Fig. 3e, red circle) and eCO_2/COR:OER systems fed with alkaline electrolyte or pure water (Fig. 3e, blue). We include previously reported CO_2R to C_2H_4 and COR to C_2H_4 electrolysers (the system boundaries are depicted in Supplementary Fig. 12, in which the syngas is produced from plastic gasification process and the CO_2 is from direct air capture process; the heat value of feedstocks and products are not considered) and included reports with advanced cathode catalysts such as bimetallic, defect-rich and molecular functionalized Cu nanostructures[4,13,18]. The lowest previously reported electrical energy cost (not including the thermal energy used for direct air capture) to produce C_2H_4 has been 134 $GJ_{electricity}$ per ton_{C2H4} (refs. 4,13), this in systems that employ alkaline electrolytes; the lowest reported in pure water has been 330 $GJ_{electricity}$ per ton_{C2H4} (ref. 15) (Fig. 3e, the detailed values for electrical and thermal energy used are included in Supplementary Table 2). The present COR:HOR system requires electrical energy 49 $GJ_{electricity}$ per ton_{C2H4} when combined with self-sustainable plastic gasification (no extra electricity input required)[36], and paths remain to lower further the electricity consumption, such as by introducing advanced catalysts. Techno-economic analysis (detail in Supplementary Note 1) highlights that this electricity consumption suggests a lowered electrified ethylene production cost (~US$1,900 per ton_{C2H4}) compared to OER coupled systems (>US$2,800 per ton_{C2H4}; Supplementary Fig. 13). Steam cracking processes have low energy cost (~12 to 54 GJ per ton_{C2H4}) (ref. 11), but the electrified system brings benefits such as a lowered projected carbon intensity (Methods provide carbon footprint analysis) of ~0.45 kg_{eqCO2} per kg_{C2H4} compared to 1–3 kg_{eqCO2} per kg_{C2H4} for steam cracking[11] (Fig. 3e).

Studies of system stability under intermittent operation

The durability of the solid-state COR:HOR MEA was evaluated and compared with COR:OER MEA. The two systems were operated at the same temperature of 55 °C to lower the cell voltage[35]. First, the system's durability was evaluated under continuous operation at 100 mA cm^{-2}. The COR:OER MEA, fed with 1.0 M NaOH as anolyte, was limited to 20 hours of stable operation, and it lost 60% of its initial FE_{C2H4} (from ~50% to ~20%) following 50 hours of operation at 55 °C (Fig. 4a, top). We observe salt deposition in the flow channel (this result not of carbonate formation, but of failure of anolyte/water management in liquid–anode systems at the more realistic operating temperature[37] (Supplementary Fig. 14)). By analysing the contact angle at the cathode GDL after the continuous operation, we found that the hydrophobicity of the GDL in COR:OER system has been compromised (Fig. 4b, middle).

In contrast, the HOR-coupled MEA retained 90% of its initial FE_{C2H4} following 80 hours of operation at 100 mA cm^{-2} at 55 °C (Fig. 4a, bottom)[37]. It maintains good hydrophobicity and water management (Fig. 4b, bottom) as required for efficient gas transport to reactive sites[35]. Nevertheless, we note that it will be important to develop strategies to provide heat removal and to retain the hydrophobicity of the GDL over extended operation.

We tested for Na^+ and PANa polymer loss, conducting inductively coupled plasma mass spectrometry and nuclear magnetic resonance (NMR) tests on both the anode and the cathode by cooling down and condensing the outlet gas streams. We found that Na^+ leaching was less than 5% Na after 70 hours at 100 mA cm^{-2} (Supplementary Fig. 15); and we detected no PANa polymer (Supplementary Fig. 16). We also obtained post-operando X-ray photoelectron spectroscopy and infrared (IR) spectroscopy and found that Na^+ remains, exclusively in the $-COO^-Na^+$ form (no –COOH—the product of Na^+ leaching—is observed

in the IR studies), following the stability test (Supplementary Fig. 17b). These results suggest that the Na^+ is substantially retained in the PANa cation-functionalized layer (details in Supplementary Fig. 6). We note that long-term reliability could be further strengthened by cation re-supply[38]. While we cannot exclude the possibility of PANa polymer loss beyond the studied operation timeframe, we note that the solubility/dispersion of PANa in water depends on its molecular weight and polymer architecture; thus one could move to higher molecular weight to increase interfacial interaction, and one could crosslink or functionalize the polymer to reduce water solubility[34,39].

When we probed performance under intermittent biasing, we found that Cu-based catalysts were prone to degradation when exposed to alkaline electrolytes before electrolyser start-up in the absence of protective reductive potential, resulting in over 60% reduction in FE_{C2H4} and ten times increase in FE_{H2} compared to the normal baseline (Supplementary Fig. 18). Although the liquid anolyte system initially delivered normal FE_{C2H4} with a careful start-up procedure with protective reductive potential, it lost >80% of its beginning-of-test FE_{C2H4} after a 2-hour rest at open circuit and showed almost no ethylene production (H_2 as main products) after an additional 12-hour rest, especially at higher operating temperature (Fig. 4c, grey; Supplementary Figs. 19 and 20). Notably, the COR:HOR system maintained its FE_{C2H4} without noticeable loss after 30 on/off intermittent cycles with 12-hour rests (Fig. 4c, blue).

To study the origins of degradation under intermittent operation, we used in situ Raman (table of peak assignments and discussion provided in Supplementary Table 3) complemented by post-operando X-ray diffraction (XRD). In the case of COR:OER (which includes a caustic anolyte), features associated with Cu oxidation are prominent after the reducing potential is removed, as indicated by the catalyst colour change and the observation of Cu (hydro)oxide peaks at 500–600 cm^{-1} (Supplementary Fig. 21, relatively weak signal due to the loss of enhancement effect from metallic Cu). This is consistent with post-operando XRD results, which show the formation of $Cu(OH)_2$ only in the case of COR:OER after the off cycles (Supplementary Fig. 22). After we re-applied the reduction potential in the COR:OER case, the C–O stretching feature at ~2,100 cm^{-1} did not recover to its initial state (Fig. 4d, grey line, where Cu–CO, Cu–OH coexist), and only the Cu–OH interaction at ~540 cm^{-1} remained (Fig. 4d, after rest; Cu–OH peak assignments and discussion provided in Supplementary Table 3). We propose that when Cu–OH coverage is high, this leads to competition for binding and militates against CO conversion to C_2H_4. These findings suggest that Cu is more vulnerable to oxidation and degradation, leading to the loss of the desired surface attributes needed for CO adsorption, when the catalyst is in contact with strong alkaline electrolyte, consistent with the Pourbaix diagram and with previous reports[15]. Nevertheless, these initial studies leave opportunities to develop operando Raman to explore intermittency-tolerant COR:HOR MEA systems in further depth.

Conclusions

We explored a suite of ionomers as solid-state cation-functionalized layer for the construction of COR:HOR solid-state system. We identified an efficient alkali cation–host, polyacrylate, which united the high ion-exchange capacity with optimized cation binding. With polyacrylate sodium as cation-functionalized layer, we documented an electricity-efficient C_2H_4 production at 1.2 V and 100 mA cm^{-2} in the COR:HOR solid-state system. These mechanistic studies and the performance of the pure-water-fed solid-state COR:HOR electrolyser suggest routes to managing electricity demand in chemicals production and compatibilizing such technologies to function with growing reliance on intermittent renewable electricity.

Methods

Materials

Methanol (99.8%), sodium hydroxide (puriss, 98–100.5%), sodium polyacrylate (PANa, average Mw ~2,100), polyacrylic acid solution (50 wt%), isopropanol (>99.5%), dimethyl sulfoxide (DMSO), deuterium oxide (D_2O, > 99.9 atom%) were all purchased from Sigma-Aldrich without further treatment. 1,1-dimethylpiperidinium chloride (Pip^+Cl^- > 98.0%) was purchased from TCI America. Copper nanoparticle catalyst (25 nm, Cu NPs) was purchased from US Research Nanomaterials Inc. Ethanol (USP/NF grade) was purchased from Commercial Alcohols. PiperION membrane (40 um), PtRu/C catalyst (50 wt% on carbon black), Freudenberg H23C3, nickel foam, platinized titanium felt, iridium oxide, carbon black (Vulcan XC-72), Sustainion XA-9 ionomer solution (5 wt%), PiperION ionomer solution (5 wt%) were purchased from Fuel Cell Store. Aemion ionomer (AP-2) power was purchased from Ionomr Innovations. Nafion D520 perfluorinated sulfonic acids resin solution (5 wt% PFSA in a mixture of lower aliphatic alcohols and water), Nafion 211 membrane were purchased from Ion Power Inc. The Ag/AgCl reference electrodes used in flow cell were purchased from CHI Instruments Inc. Semiconductor grade CO (99.997%) and ultrahigh-purity hydrogen (H_2) were purchased from Airgas. Ultrapure water (18.2 MΩ from MiliQ) was used to prepare all the solutions and electrolytes. The electrolyser cell and humidified system were purchased from Fuel Cell Technologies.

Electrode preparation

To prepare the cathodes that were used in flow cell and membrane-electrode assembly (MEA), 20 mg Cu-based catalysts, 2 ml methanol and 60 µl Nafion solution were added into a 20 ml vial. The mixture was sealed and sonicated in a water bath for 1–3 hours (the temperature of the water bath was kept below 30 °C. The solution was then sprayed onto a 3 cm × 3 cm gas diffusion electrode (Freudenberg H23C3). The final catalyst loading was controlled to be 1.5 ~ 2 mg cm^{-2}. After drying in an ambient environment overnight, the gas diffusion electrode was cut into 1 cm × 1 cm for further use.

To prepare the catalyst-coated membrane for anode hydrogen oxidation reaction in MEA, 50 mg 50% PtRu/C, 360 mg Nafion D520 solution and 25 ml mixture of water and isopropanol (ratio of 1:4) were added into a 35 ml vial. The mixture was sealed and sonicated for 2 hours. It was then sprayed onto a 6 cm × 10 cm Nafion 211 membrane. The final catalyst loading was controlled around 0.2 mg_{PGM} cm^{-2}. The electrode was cut into 1.5 cm × 1.5 cm pieces for further use.

The anode for oxygen-evolution reaction in MEA was Ni foam or IrO_x-coated platinized titanium felt purchased from Fuel Cell Store.

Preparation of cation-functionalized layer on membrane

To prepare the carbon solution, 10 mg carbon black, 10 ml methanol, and 100 mg of 5 wt% Nafion D520 solution were added into a 20 ml vial. The vial was then sealed and sonicated in a water bath for 1–3 hours, while the temperature of the water bath was kept below 30 °C. Next, the cation-containing ionomer solutions were prepared by mixing the chosen ionomer (for example, Nafion, polyacrylic acid) with the alkaline solution (for example, NaOH) to incorporate alkali cations or by adding the commercial ionomer solution (for example, PiperION, Aemion, Sustainion XA-9). Then 1 ml of the carbon solution was added into 1 ml of the cation-containing ionomer solution, and the resulting mixture was uniformly sprayed onto a 1.5 cm × 1.5 cm PiperION membrane.

Flow cell

The flow cell tests were conducted in a three-chamber PTFE flow cell. The active area had a size of 1 cm × 1 cm. Ag/AgCl in saturated KCl (CHI instrument Inc.) was used as the reference electrode. A piece of Pt mesh with a size of 0.6 cm × 1 cm was used as the counter electrode. The catholyte and anolyte were separated by an anion-exchange membrane. During operation, the CO flow rate was set to 20 sccm, catholyte and anolyte were supplied separately by peristaltic pumps.

MEA

To assemble the MEA, the Cu electrode was cut into 1 cm × 1 cm pieces. The cathode electrode was placed on the cathode plate (stainless

steel) with the catalyst side facing upward. A piece of 2 cm × 2 cm anion-exchange membrane or cation-functionalized membrane was put on top of the cathode with the cation-functionalized layer facing the cathode. Then a catalyst-coated membrane was put on top of the anion-exchange membrane with the catalyst side facing another gas diffusion electrode placed on the anode plate (Titanium). To prevent leakage, two PTFE gaskets with a thickness of 0.01 inch were placed between the cathodic plate and membrane, membrane and anodic plate, respectively. During operation, humidified CO and H_2 were supplied to the cathode and anode, respectively, and the flow rates were controlled by digital mass flow controllers (Alicat Scientific). In the case of COR:OER, liquid electrolyte (1 M NaOH or pure water) was pumped through the anode with a peristaltic pump, and the pure water was flown in a single-path mode to avoid the impact from dissolved alkali cations in the electrolyte.

Electrochemical measurement

All the electrochemical measurements were conducted using an electrochemical station (BioLogic) connected to a current booster (20 V, 20 A). The COR performance was evaluated in galvanostatic mode at a cell temperature of ~55 °C and feed gases humidity of around 100%. The intermittent stability test was conducted by repeatedly start and stop the cell with required period (2 or 12 hours, depicted in Supplementary Fig. 19). The data collection was conducted after the cell has been stabilized at each current density.

Impedance measurements

The impedance spectra were measured using frequencies from 10^5 to 1 Hz with an amplitude of 0.1 mA at different current density in a flow cell, in which the Cu catalysts were reduced and activated at −50mA cm^{-2} for 10 min to get a stable EIS measurement. The CO flow rate (20 sccm) and electrolyte flow rate (20 rpm) were kept the same as the COR performance test in the flow cell during the impedance measurement. Equivalent circuits were fitted to the data using EC-lab software version 11.52.

COR product analysis

The gas phase products were collected by gas-tight calibrated syringe and analysed by a calibrated gas chromatography (PerkinElmer) equipped with a thermal-conductivity detector for the detection of H_2, CO and a flame-ionization detector for the detection of ethylene and methane. The Faradaic efficiency (FE) of a gas product can be calculated via equation (1):

$$\mathrm{FE} = \frac{nF\upsilon c}{iV_m} \tag{1}$$

where n is the number of electrons transferred during the reaction (8 for ethylene, 6 for methane, 2 for hydrogen), F is the Faraday constant (96,485 C mol^{-1}), υ is the flow rate of CO, c is the concentration of the product in the outlet in parts per million (ppm), i is the total current and V_m is the unit molar volume of gas.

Liquid products were analysed by ^{1}H NMR spectroscopy (400 MHz Bruker Avance III HD Nanobay 400 system) with water suppression. Dimethyl sulfoxide (DMSO) was used as an internal standard and D_2O was used as lock solvent.

Materials characterization

The transmission electron microscopy and atomic resolution high-angle annular dark-field scanning transmission electron microscopy images were taken from aberration-corrected JEOL GrandArm 200 microscope operated at an acceleration voltage of 200 kV. A probe convergence angle of 20 mrad was used. The XRD measurements were conducted on STOE STADI-P using Cu K-α radiation (λ = 0.15406 nm). Contact angles were automatically measured and averaged from VCA Optima XE.

In situ Raman spectroscopy

The in situ Raman spectroscopy was conducted in a customized flow cell with an epi-illumination configuration. Cu catalysts were directly used due to their known surface enhancement effect in Raman spectroscopy. To study the cation effect on COR, electrolytes with different cationic groups were used (1 M PANa, 1 M Pip^+Cl^-, 1 M NaOH). Lasers at 785 nm and 633 nm were used as the excitation sources for COR intermediate and interfacial water detection with a laser power of 0.1%. The scattered Raman light was collected by a water immersion objective (Leica, HC APO L 63x/0,90 W U-V-I). Each time before the measurement, the spectrometer was calibrated by a standard silicon sample. During operation, CO gas flowed through the gas chamber that was located on the back of GDL. The Raman spectrum was collected after the current response was stabilized at each potential. To study the impact of intermittent operation, a series of Raman spectra was collected after the electrochemical cell was turned off and after re-started the cell at reductive potentials.

Density functional theory calculations

All density functional theory (DFT) calculations were performed using the ORCA v5.0 software package[40]. Structural optimizations employed the Perdew-Burke-Ernzerhof[41] functional together with the Grimme–Becke–Johnson D3 empirical correction[42] for London dispersion forces. The def2-TZVPD basis set[43,44], which includes polarization functions and diffuse functions for charged species, was applied to all atoms. An ultra-fine integration grid was used throughout. Implicit solvation was implemented via the conductor-like polarizable continuum model (CPCM)[45], parameterized to represent water.

Frequencies were computed to predict thermochemical properties including zero-point energies, enthalpies (H) and entropies (S). By default, entropies are evaluated within the quasi-harmonic approximation, treating all modes as ideal-gas-like oscillators. This approach does not capture the restricted vibrational and rotational motions imposed by surrounding solvent molecules. To address this limitation, translational and rotational entropies of small species (H_2O, Na, OH) were reduced by 54% (ref. 46). Accordingly, Gibbs free energies (G) at 298.15 K were computed as:

$$G = H - T \times (0.46 \times (S_{\mathrm{trans}} + S_{\mathrm{rot}}) + S_{\mathrm{vib}}) \tag{2}$$

where S_{trans}, S_{rot} and S_{vib} denote translational, rotational and vibrational entropy contributions, respectively.

The Na^+ dissociation free energies (ΔG_{diss}) were computed according to equation (3):

$$\Delta G_{\mathrm{diss}} = G_{X^-} + G_{\mathrm{Na}^+-6\,\mathrm{H_2O}} - G_{\mathrm{Na}-X} - 6 \times G_{\mathrm{H_2O}} \tag{3}$$

$G_{\mathrm{Na}-X}$ is the free energy of the cation–anion coupled system. G_{X^-} is the free energy of this system with a Na^+ removed, rendering the remaining motif negatively charged. $G_{\mathrm{Na}^+-6\,\mathrm{H_2O}}$ is the free energy of the Na^+ surrounded by a solvation shell of six water molecules. For the case of NaOH, the G_{X^-} is the OH^- anion surrounded by four strongly hydrogen-bonded water molecules. ΔG_{diss} is summarized in Supplementary Fig. 6.

Energy cost, techno-economic and carbon footprint analyses

Energy cost analysis and carbon footprint analysis were conducted to evaluate the economic feasibility and prospective environmental impacts of the syngas upgrading system. For the electricity input, an efficiency factor of 95.2% was used to account for the fuel cycle energy used for electricity based on the GREET database. In electrolysis approaches, the greenhouse gas (GHG) emissions are dominated by the carbon footprint of electric energy. We use a carbon footprint value of 0.0078 kg_{eqCO2} MJ_e^{-1} to represent an average of solar (photovoltaic) and wind renewable electricity according to the National Renewable Energy

Laboratory report[47]. The energy analysis and carbon footprint for industrial processes, including MTO and steam cracking, was obtained from a published work[11]. The syngas was assumed to be produced from a reported self-sustainable integrated plastic gasification process[36] and separated into CO and H_2 for further use in the COR-HOR coupled electrolyser. For CO_2R–C_2H_4 and the cascade CO_2–CO–C_2H_4 process, the upstream CO_2 air capture energy cost is assumed to be 8 GJ per ton_{CO2} (ref. 48), powered by the high-grade heat from natural gas-fired calciner. The carbon footprint for using high-grade heat from natural gas combustion is 56.1 kg_{eqCO2} GJ^{-1} (ref. 49). The CO_2–CO process is assumed to be through a solid-oxide electrolyser cell with 90% FE and an energy cost of 19.3 GJ per ton_{CO2} (TOPSOE). A pressure swing adsorption process is used for all the required gas separation processes at an energy cost of 0.25 kWh m^{-3} (ref. 50). The syngas was assumed to be produced from a reported self-sustainable integrated plastic gasification process[36] (in which no extra electricity input was required) and separated into CO and H_2 for further use in the COR-HOR coupled electrolyser. The result shows that when using a typical flue gas capture ratio of 90%, the carbon footprint associated with the waste plastic treatment—gasification—syngas clean-up is 0.035 kg_{CO2} per kg_{syngas}, which eventually translates to 0.14 kg_{CO2} per $kg_{ethylene}$, and is similar to the reported value of 0.10 kg_{CO2} per $kg_{ethylene}$ (0.027 kg_{CO2} per kg_{syngas}) (ref. 51).

The techno-economic analysis was developed and modified based on previously reported models[50,52]. The analysis was based on an ethylene production rate of 100,000 kg d^{-1}. The cost of electrolyser was projected based on Department of Energy Hydrogen Analysis (DOE H2A) model for central grid electrolysis; the electrolyser capital cost is projected to be US$250.25 kW^{-1} at 0.175 A cm^{-2} and 1.75V (ref. 50), similar to the operation condition of our syngas upgrading electrolyser. The installation factor was assumed to be 1.2, and the balance of plant capital cost is 35% of the total cost while the electrolyser stack is 65% of total cost. The capital cost of the pressure swing adsorption (PSA) system is based on previous reference (1.99 M for 1,000 m^{-3} h^{-1}) (ref. 50), with a PSA capacity scaling factor of 0.7. The capital expenditure (CapEx) for a 5-MW solid oxide electrolyzer cell (SOEC) system was about €2,000 kW^{-1} in 2020. Projections suggest that this cost will decrease to €1,000 kW^{-1} by 2030[53]. Here we use a CapEx of US$1,250 kW^{-1}, a cell voltage of 1.5 V at 1 A cm^{-2} for SOEC electrochemical system.

Here the capital recovery factor is based on a discount rate (i, assumed to be 5%), the equipment lifetime (here we use a conservative estimation of 20 years).

We adopted a conservative renewable electricity cost of US$0.05 kWh^{-1} (ref. 54); a syngas feedstock cost of US$0.26 kg^{-1} from waste gasification[55]; an air captured CO_2 cost of US$0.23 kg^{-1} (an average from US$0.125–0.335 kg^{-1}) based on an International Energy Agency report[48].

Detailed discussion and calculation process of the techno-economic analysis is provided in Supplementary Note 1.

Data availability

All data are available in the main text or the supplementary materials. Source data are provided with this paper.

References

1. Ozden, A. et al. Carbon-efficient carbon dioxide electrolysers. *Nat. Sustain.* **5**, 563–573 (2022).
2. Kim, S. W., Kim, Y. T., Tsang, Y. F. & Lee, J. Sustainable ethylene production: recovery from plastic waste via thermochemical processes. *Sci. Total Environ.* **903**, 166789 (2023).
3. Ghanta, M., Fahey, D. & Subramaniam, B. Environmental impacts of ethylene production from diverse feedstocks and energy sources. *Appl. Petrochem. Res.* **4**, 167–179 (2014).
4. Liang, Y. et al. Efficient ethylene electrosynthesis through C–O cleavage promoted by water dissociation. *Nat. Synth.* **3**, 1104–1112 (2024).
5. *Ethylene—Global Strategic Business Report* (Global Industry Analysts, 2025).
6. Leonzio, G., Chachuat, B. & Shah, N. Towards ethylene production from carbon dioxide: economic and global warming potential assessment. *Sustain. Prod. Consum.* **43**, 124–139 (2023).
7. KPMG. *Electricity Generation Worldwide from 1990 to 2023* (Energy and Resources Institute, 2024).
8. *Renewables 2024* (IEA, 2024).
9. Energy Analysis and Environmental Impacts Division. *United States Data Center Energy Usage Report* (Lawrence Berkeley National Laboratory, 2024).
10. Yu, H. et al. Direct production of olefins from syngas with ultrahigh carbon efficiency. *Nat. Commun.* **13**, 5987 (2022).
11. Ren, T., Patel, M. K. & Blok, K. Steam cracking and methane to olefins: energy use, CO_2 emissions and production costs. *Energy* **33**, 817–833 (2008).
12. *Light Olefins Market Size, Share, Growth, and Industry Analysis, By Type (Ethylene, Propylene), By Application (Chemical Commodities, Refinery), Regional Insights and Forecast to 2032* (B. R. Insights, 2025).
13. Wu, H. et al. Selective and energy-efficient electrosynthesis of ethylene from CO_2 by tuning the valence of Cu catalysts through aryl diazonium functionalization. *Nat. Energy* **9**, 422–433 (2024).
14. Fang, W. et al. Durable CO_2 conversion in the proton-exchange membrane system. *Nature* **626**, 86–91 (2024).
15. Li, W. et al. Bifunctional ionomers for efficient co-electrolysis of CO_2 and pure water towards ethylene production at industrial-scale current densities. *Nat. Energy* **7**, 835–843 (2022).
16. Weiß, A. et al. Impact of intermittent operation on lifetime and performance of a PEM water electrolyzer. *J. Electrochem. Soc.* **166**, F487 (2019).
17. Speck, F. D. & Cherevko, S. Electrochemical copper dissolution: a benchmark for stable CO_2 reduction on copper electrocatalysts. *Electrochem. Commun.* **115**, 106739 (2020).
18. She, X. et al. Pure-water-fed, electrocatalytic CO_2 reduction to ethylene beyond 1,000 h stability at 10 A. *Nat. Energy* **9**, 81–91 (2024).
19. Fan, M. et al. Cationic-group-functionalized electrocatalysts enable stable acidic CO_2 electrolysis. *Nat. Catal.* **6**, 763–772 (2023).
20. Miao, R. K. et al. Electroosmotic flow steers neutral products and enables concentrated ethanol electroproduction from CO_2. *Joule* **5**, 2742–2753 (2021).
21. Shayesteh Zeraati, A. et al. Carbon- and energy-efficient ethanol electrosynthesis via interfacial cation enrichment. *Nat. Synth.* **4**, 75–83 (2024).
22. Zhao, Y. et al. Conversion of CO_2 to multicarbon products in strong acid by controlling the catalyst microenvironment. *Nat. Synth.* **2**, 403–412 (2023).
23. Xu, Y., Xia, Z., Gao, W., Xiao, H. & Xu, B. Cation effect on the elementary steps of the electrochemical CO reduction reaction on Cu. *Nat. Catal.* **7**, 1120–1129 (2024).
24. Malkani, A. S. et al. Understanding the electric and nonelectric field components of the cation effect on the electrochemical CO reduction reaction. *Sci. Adv.* **6**, eabd2569 (2020).
25. Monteiro, M. C. O., Dattila, F., López, N. & Koper, M. T. M. The role of cation acidity on the competition between hydrogen evolution and CO_2 reduction on gold electrodes. *J. Am. Chem. Soc.* **144**, 1589–1602 (2022).
26. Gunathunge, C. M., Li, J., Li, X. & Waegele, M. M. Surface-adsorbed CO as an infrared probe of electrocatalytic interfaces. *ACS Catal.* **10**, 11700–11711 (2020).

27. Lee, S. Y. et al. Probing cation effects on *CO intermediates from electroreduction of CO_2 through operando Raman spectroscopy. *J. Am. Chem. Soc.* **145**, 23068–23075 (2023).
28. Resasco, J. et al. Promoter effects of alkali metal cations on the electrochemical reduction of carbon dioxide. *J. Am. Chem. Soc.* **139**, 11277–11287 (2017).
29. Tran, B. & Goldsmith, B. R. Theoretical investigation of the potential-dependent CO adsorption on copper electrodes. *J. Phys. Chem. Lett.* **15**, 6538–6543 (2024).
30. García de Arquer, F. P. et al. CO_2 electrolysis to multicarbon products at activities greater than 1 A cm^{-2}. *Science* **367**, 661–666 (2020).
31. Whitney, D. C. & Diamond, R. M. Ion-exchange studies in concentrated solutions. I. The alkali cations with a sulfonic and a carboxylic acid resin. *Inorg. Chem.* **2**, 1284–1295 (1963).
32. Wei, Y., Shi, Y., Chen, Y., Xiao, C. & Ding, S. Development of solid electrolytes in Zn–air and Al–air batteries: from material selection to performance improvement strategies. *J. Mater. Chem. A* **9**, 4415–4453 (2021).
33. Song, Z. et al. Poly(acrylic acid)-based composite gel polymer electrolytes with high mechanical strength and ionic conductivity toward flexible zinc–air batteries with long cycling lifetime. *ACS Appl. Mater. Interfaces* **14**, 49801–49810 (2022).
34. Zhang, G. et al. Construction of alkaline gel polymer electrolytes with a double cross-linked network for flexible zinc–air batteries. *ACS Appl. Polym. Mater.* **5**, 3622–3631 (2023).
35. Zhao, J. Y. et al. A focus on the electrolyte: realizing CO_2 electroreduction from aqueous solution to pure water. *Chem Catal.* **3**, 100471 (2023).
36. Koppala, B. C. N. et al. Comparative assessment on thermo-chemical conversion of different waste plastics to value added syngas: thermodynamic investigation. *Environ. Dev. Sustain.* **27**, 26801–26821 (2025).
37. Pelzer, H. M., Kolobov, N., Vermaas, D. A. & Burdyny, T. Scaling and heating will drive low-temperature CO_2 electrolysers to operate at higher temperatures. *Nat. Energy* **10**, 549–556 (2025).
38. Endrődi, B. et al. Operando cathode activation with alkali metal cations for high current density operation of water-fed zero-gap carbon dioxide electrolysers. *Nat. Energy* **6**, 439–448 (2021).
39. Liu, M. & Guo, T. Preparation and swelling properties of crosslinked sodium polyacrylate. *J. Appl. Polym. Sci.* **82**, 1515–1520 (2001).
40. Neese, F. The ORCA program system. *WIREs Comput. Mol. Sci.* **2**, 73–78 (2012).
41. Perdew, J. P., Burke, K. & Ernzerhof, M. Generalized gradient approximation made simple. *Phys. Rev. Lett.* **77**, 3865 (1996); erratum *Phys. Rev. Lett.* **78**, 1396 (1997).
42. Grimme, S., Antony, J., Ehrlich, S. & Krieg, H. A consistent and accurate ab initio parametrization of density functional dispersion correction (DFT-D) for the 94 elements H-Pu. *J. Chem. Phys.* **132**, 154104 (2010).
43. Weigend, F. & Ahlrichs, R. Balanced basis sets of split valence, triple zeta valence and quadruple zeta valence quality for H to Rn: design and assessment of accuracy. *Phys. Chem. Chem. Phys.* **7**, 3297–3305 (2005).
44. Rappoport, D. & Furche, F. Property-optimized Gaussian basis sets for molecular response calculations. *J. Chem. Phys.* **133**, 134105 (2010).
45. Klamt, A. & Schüürmann, G. COSMO: a new approach to dielectric screening in solvents with explicit expressions for the screening energy and its gradient. *J. Chem. Soc. Perkin Trans.* **2**, 799–805 (1993).
46. Wertz, D. H. Relationship between the gas-phase entropies of molecules and their entropies of solvation in water and 1-octanol. *J. Am. Chem. Soc.* **102**, 5316–5322 (1980).
47. *Life Cycle Greenhouse Gas Emissions from Electricity Generation: Update* (National Renewable Energy Laboratory, 2021); https://docs.nrel.gov/docs/fy21osti/80580.pdf
48. *Direct Air Capture 2022* (IEA, 2022).
49. Pörtner, H.-O. et al. (eds.) *Annex I: Global to Regional Atlas* (IPCC, 2014).
50. Jouny, M., Luc, W. & Jiao, F. General techno-economic analysis of CO_2 electrolysis systems. *Ind. Eng Chem. Res.* **57**, 2165–2177 (2018).
51. Ramos, A., Teixeira, C. A. & Rouboa, A. Assessment study of an advanced gasification strategy at low temperature for syngas generation. *Int. J. Hydrogen Energy* **43**, 10155–10166 (2018).
52. Liu, H. et al. Hierarchically porous carbon supports enable efficient syngas production in electrified reactive capture. *Energy Environ. Sci.* **18**, 6628–6640 (2025).
53. Hauch, A. et al. Recent advances in solid oxide cell technology for electrolysis. *Science* **370**, eaba6118 (2020).
54. *Lazard Releases 2025 Levelized Cost of Energy+ Report* (Lazard, 2025).
55. Park, M.-J., Yun, S., Jeong, D.-W. & Won, W. Upcycling municipal solid waste: scenario-based techno-economic evaluation and life cycle assessment. *Energy* **329**, 136786 (2025).

Acknowledgements

This work received support from The Dow Chemical Company under reference number 223029BF (B.P., X.M., K.X., E.H.S.). This work made use of the Northwestern University Micro/Nano Fabrication facility of Northwestern University's Atomic and Nanoscale Characterization Experimental Center, which has received support from the Soft and Hybrid Nanotechnology Experimental Resource (National Science Foundation (NSF) ECCS-2025633), the International Institute for Nanotechnology and Northwestern's Materials Research Science and Engineering Center programme (NSF DMR-2308691). The crystallography and NMR support from Integrated Molecular Structure Education and Research Center (RRID:SCR_017874) at Northwestern are also acknowledged. We thank J. Barton, D. Hickman, S. S. Bhargava (The Dow Chemical company) for helpful discussion. We also thank J. O'Donnell-Sloan and J. B. Dunn (Northwestern University) for their discussion and support for our energy cost analysis.

Author contributions

E.H.S., K.X. and M.G.K. supervised this project. B.P. conceived the idea of this project. B.P. and Z.L. designed electrochemical devices and carried out electrochemical measurements. X.M. carried out material synthesis and XRD, NMR and ICP measurements. W.N. and B.P. performed the Raman experiments. Z.L., H.P. and B.P. conducted techno-economic and life-cycle analysis; B.P. and A.H.S. conducted the EIS and data analysis. C.B.M. performed DFT calculations. J.H. and A.M. carried out contact angle measurements; B.P., Z.L. and E.H.S. co-wrote the paper with input from all the co-authors. All authors contributed to the discussion of the results and the final paper preparation.

Competing interests

B.P., E.H.S. and K.X. have filed a US provisional patent application (63/797,144) based on this work. The other authors declare no competing interests.

Additional information

Supplementary information The online version contains supplementary material available at https://doi.org/10.1038/s41560-026-01990-2.

Correspondence and requests for materials should be addressed to Ke Xie or Edward H. Sargent.

Peer review information *Nature Energy* thanks Guiyan Zang and the other, anonymous, reviewer(s) for their contribution to the peer review of this work.